Chemical shift anisotropy selective inversion

Citation: Caporini, Marc A., Christopher J. Turner, Anthony Bielecki, and Robert G. Griffin. "Chemical shift anisotropy selective inversion." Journal of Magnetic Resonance 200, no. 2 (October 2009): 233-238.

As Published: http://dx.doi.org/10.1016/j.jmr.2009.07.003

Publisher: Elsevier B.V.

Persistent URL: http://hdl.handle.net/1721.1/82061

Version: Author's final manuscript: final author's manuscript post peer review, without publisher's formatting or copy editing

Published in final edited form as:
J Magn Reson. 2009 October ; 200(2): 233–238. doi:10.1016/j.jmr.2009.07.003.

Chemical Shift Anisotropy Selective Inversion*

Marc. A. Caporini, **Christopher. J. Turner**, **Anthony Bielecki**, and **Robert G. Griffin**
Department of Chemistry and Francis Bitter Magnet laboratory, Massachusetts Institute of Technology, Cambridge Massachusetts 02139

Abstract

Magic Angle Spinning (MAS) is used in solid-state NMR to remove the broadening effects of the chemical shift anisotropy (CSA). In this work we investigate a technique that can reintroduce the CSA in order to selectively invert transverse magnetization. The technique involves an amplitude sweep of the radio frequency field through a multiple of the spinning frequency. The selectivity of this inversion mechanism is determined by the size of the CSA. We develop a theoretical framework to describe this process and demonstrate the CSA selective inversion with numerical simulations and experimental data. We combine this approach with cross polarization (CP) for potential applications in multi-dimensional MAS NMR.

1. Introduction

Almost all approaches to selective excitation are related to the pioneering work of Alexander [1] who devised a method of pulsed excitation of one resonance while leaving a chemically shifted neighbor unaffected (subjected to rotation by 2π radians). Although modern selective inversion methods use amplitude- and/or phase-modulated pulses, the selectivity is nevertheless based upon differences in the chemical shift. In this work we discuss a magic-angle spinning (MAS) NMR experiment in which the selection criterion is the anisotropy of the chemical shielding, rather than the chemical shift itself.

The chemical shift anisotropy (CSA) is rotationally averaged at MAS frequencies higher than the span of the CSA. However, the CSA interaction can be reintroduced with rotary resonance recoupling by matching the RF field strength to a multiple of the MAS frequency [2]. When the resonance condition is met with a constant value of $\omega_1 = n\omega_r$ ($n = 1, 2$), the CSA is said to be recoupled, and for a polycrystalline sample, the superposition of different precession frequencies causes a rapid decay of the transverse magnetization [2]. Here, we examine the effect of an amplitude sweep of the RF field to produce a gradual passage through the CSA recoupling condition, a technique that has previously been used in the determination of small CSA values [3].

This paper is organized as follows. In Section 2 we outline the theoretical framework for CSA selective inversion. In Section 3 we present numerical simulations, which relate the efficiency of inversion to parameters such as the anisotropy, spinning frequency, and the duration of the RF amplitude ramp. In section 4 we present experimental data to demonstrate some of these effects. Finally, in section 5 we show that CSA selective inversion can be combined with

ramped cross-polarization, especially at such high MAS frequencies that the cross-polarization matching condition can be close to one of the rotary resonance recoupling conditions [4,5].

2. Theory

The pulse sequence starts with a period of cross-polarization (CP) followed by a period during which the ^{13}C RF amplitude is swept through a CSA recoupling condition as shown in Figure 1b. Proton decoupling is applied during the ^{13}C RF amplitude sweep, at a power level high enough to avoid depolarization effects during this period [6, 7].

We shall describe the process of creating an adiabatic passage through rotary resonance via average Hamiltonian theory (AHT). For simplicity, we assume a single spin and consider only the RF irradiation and the CSA terms of the Hamiltonian. We restrict the RF amplitude variation, $\omega_1(T)$, to be slow relative to the MAS rotation so that the Hamiltonian in the rotating frame takes the form of Equation (1).

$$H(t,T)=\omega_1(T)I_x+\sum_{k=-2}^{2}c_k e^{-ik\omega_r t}I_z \tag{1}$$

The Fourier expansion parameters, c_k, of the modulated chemical shift depend upon the CSA parameters and the orientation of the CSA tensor in the rotor frame and are given by Equation (2).

$$c_k=\sqrt{\tfrac{2}{3}}\omega_0\sum_{k'=-2}^{2}\rho_{2.k'}D^2_{k',k}(\alpha,\beta,\gamma)D^2_{k,0}(0,\theta_m,0) \tag{2}$$

where ω_0 is the Larmor frequency, θ_m is the magic angle, and (α, β, γ) are the Euler angles that transform the CSA principal axis frame into the rotor frame. $D^2_{k',k}(\alpha,\beta,\gamma)$ are elements of the second-rank Wigner rotation matrix and $\rho_{2.k'}$ are the irreducible spherical tensor components of the CSA interaction in the principal axis frame, defined by $\rho_{2,0}=\sqrt{\tfrac{3}{2}}(\delta_{zz}-\delta_{iso})=\sqrt{\tfrac{3}{2}}\delta, \rho_{2,\pm1}=0$, and $\rho_{2,\pm2}=(\delta_{yy}-\delta_{xx})/2=\delta\eta/2$ where δ_{xx}, δ_{yy} and δ_{zz} are the principal values, and δ_{iso}, δ, η are the isotropic part, the anisotropy, and asymmetry parameter of the CSA tensor, respectively [8].

In a doubly rotating frame, defined by the additional transformation operator $\boldsymbol{R = e^{-in\omega_{rt}I_x}}$, the Hamiltonian becomes:

$$H_R(T,t)=\Delta\omega_1(T)I_x+\frac{1}{2}\sum_{k=-2}^{2}c_k e^{-ik\omega_r t}((I_z+iI_y)e^{in\omega_r t}+(I_z-iI_y)e^{-in\omega_r t}) \tag{3}$$

where $\Delta\omega_1(T)=\omega_1(T)-n\omega_r$. The zeroeth order average for $n = 1, 2$ is given by Equation (4).

$$\tilde{H}_0(T)=\Delta\omega_1(T)I_x+(\tfrac{c_{-n}-c_n}{2i})I_y+(\tfrac{c_{-n}+c_n}{2})I_z \tag{4}$$

The expression $[(c_{-n} - c_n)/2i]I_y + (c_{-n} + c_n)/2]I_z$ defines the effective recoupling axis for each crystallite orientation (α,β,γ) whose magnitude, c_{eff}, for $n = 1$ and $n = 2$ is given in Equations 5 and 6, respectively. Since each crystallite is independent we arbitrarily rotate the recoupling axis such that it is aligned along I_z as shown in Figure 1.

For n=1,

$$c_{eff}=\omega_0\delta\sin\theta_m\cos\theta_m\sqrt{(\tfrac{\eta}{4}d^2_{2,-1}(\beta)\cos(2\alpha)+\sqrt{\tfrac{3}{2}}d^2_{1,0}(\beta))(\tfrac{\eta}{2}d^2_{2,1}(\beta)\cos(2\alpha)+\sqrt{\tfrac{3}{2}}d^2_{1,0}(\beta))} \quad (5)$$

For n= 2,

$$c_{eff}=\frac{\omega_0\delta\sin^2\theta_m}{2}\sqrt{(\tfrac{\eta}{4}d^2_{2,-2}(\beta)\cos(2\alpha)+\sqrt{\tfrac{3}{2}}d^2_{2,0}(\beta))(\tfrac{\eta}{4}d^2_{2,2}(\beta)\cos(2\alpha)+\sqrt{\tfrac{3}{2}}d^2_{2,0}(\beta))} \quad (6)$$

To estimate the size of the c_{eff} for a given δ we simplify the expressions by assuming $\eta = 0$ and calculate the scaling factors for the maximum and powder average values fo r both $n = 1$ and $n = 2$ such that c_{eff} = (scaling factor) $\omega_0\delta$. For $n = 1$, the maximum is $\sqrt{2}/4$ and the powder average is $\sqrt{2}/6$, and for $n = 2$, the maximum is $\sqrt{6}/8$ and the powder average is $\sqrt{6}/12$. A non-zero η results in minor deviations from the scaling factors listed. These simplified calculations give some insight into the size of the interaction and general dynamics of an adiabatic CSA inversion; however, the experimentally observed behavior is an average of many individual crystallite trajectories with varying c_{eff}. For this reason we perform numerical simulations in the following section, which better approximate the expected behavior.

In order to adiabatically sweep the Hamiltonian through the recoupling axis we must satisfy two conditions: first minimize the angle of the initial and final projections of the spin polarization onto the Hamiltonian and second ensure the angular sweep rate of the Hamiltonian is slow enough to be adiabatic. The first condition is satisfied when $\Delta\omega_1(\pm\tau) \geq 5\boldsymbol{c_{eff}}$[9]. The second condition is determined by the angular sweep rate ($d\theta/dT$) of the Hamiltonian near the recoupling axis [10]. The adiabaticity factor $\boldsymbol{Q}(\boldsymbol{T})=\frac{\boldsymbol{c_{eff}}}{\boldsymbol{d\theta/dT}}$ must be greater than or equal to 1 at all times during the RF ramp for the process to be adiabatic. For a linearly ramped RF field the angular velocity of the Hamiltonian is the greatest at the recoupling condition, therefore, if the process is adiabatic at the recoupling condition such that $\boldsymbol{Q}(0)\geq 1$ then the process will be adiabatic for the entire ramp. For a linear amplitude ramp with ramp rate r, the adiabaticity factor then becomes: $\boldsymbol{Q}(0)=\frac{\boldsymbol{c^2_{eff}}}{\boldsymbol{r}}$.

For the following discussion, we will detail the construction of an adiabatic ramp through the $n = 2$ rotary resonance condition that selectively inverts a spin with c_{eff} of 2 kHz while leaving one of 0.5 kHz unchanged. We choose the total RF ramp width to be ω_r symmetrically bracketing the recoupling condition ($1.5\omega_r \leq \omega_1 \leq 2.5\omega_r$) so that we have the widest possible ramp without approaching the $n = 1$ recoupling condition. In order to minimize the projection angles we must choose $\omega_r > 10\ c_{eff}$ = 20 kHz. To satisfy the adiabatic condition for c_{eff} = 2 kHz, the ramp rate $r = \omega_r/\Delta T$ must be $\leq \boldsymbol{c^2_{eff}}$ so the ramp time, ΔT, becomes, $\Delta T > \omega_r/\boldsymbol{c^2_{eff}} = 5$ ms. In a similar fashion one can calculate the minimum ramp time necessary for adiabatic inversion for c_{eff} = 0.5 kHz to be 80 ms. The 5 ms ramp is far from adiabatic for

the smaller-CSA spin. To some approximation, that site effectively experiences a spin-locking field along $\pm I_x$ over most of the ramp, with the passage through the recoupling condition acting as a small flip angle pulse, which results in a small loss of the spin-locked polarization.

At the $n = 1$ condition, the CSA tensor, the homonuclear [11], and the heteronuclear dipolar coupling tensor are all recoupled whereas at the $n = 2$ condition only the CSA tensor and the heteronuclear dipolar-coupling tensor are reintroduced [12]. This means that the $n = 1$ recoupling condition becomes very complicated and is unlikely to be useful except in situations where homonuclear dipolar couplings are negligible. Therefore, we restrict the remainder of the discussion to the $n = 2$ condition.

At the $n = 2$ condition, CSA and heteronuclear dipolar couplings are simultaneously recoupled. If the dipolar interaction is much smaller than the CSA, it amounts to only a slight perturbation of the larger CSA tensor. Dipolar coupling constants for directly bonded ^{13}C-^{15}N pairs range from approximately 1 to 2 kHz. For ^{13}C-^{14}N pairs, the larger spin of ^{14}N, $I = 1$, together with the smaller gyromagnetic ratio yield dipolar effects roughly comparable in magnitude. These dipolar couplings are smaller than most ^{13}C CSAs at high field and, more significantly, are smaller than the differences between large and small ^{13}C CSAs (e.g., between carbonyl and aliphatic), and therefore do not significantly affect the site-specific selectivity of CSA inversion.

For this reason, ^{15}N decoupling was not utilized during the CSA recoupling interval in this work. However, experiments involving selective inversion of ^{13}C sites with small CSA would likely require both ^{15}N labeling, to avoid ^{14}N-^{13}C couplings, together with ^{15}N decoupling. In such an experiment, the RF levels on ^{1}H, ^{13}C, and ^{15}N must be chosen with care to avoid interfering recoupling conditions such as CP and TSAR [13].

In the experimental data presented in this article, ^{1}H decoupling was accomplished by 100 kHz CW irradiation to avoid cross polarization/depolarization effects. In the absence of ^{1}H RF irradiation, the $n = 1$ and $n = 2$ conditions would recouple the very strong ^{1}H-^{13}C dipolar interaction (~25 kHz) and inversion with CSA selectivity would be impossible.

3. Numerical Simulations

Although the expressions derived in the previous section provide theoretical insight into the spin dynamics of CSA selective inversion, we believe it helpful to examine numerical simulations of the relationship between the CSA, the experimental parameters and the efficiency of inversion. The simulations were generated with SPINEVOLUTION 3.3.3 with powder averaging over 300 triplets of the (α, β, γ) Euler angles [14]. The simulations ignore the effects of relaxation, but include the effects of ±10% RF inhomogeneity. Since the major parameters that affect the efficiency of CSA selective inversion are the MAS frequency and the RF power level, both of which are conveniently described in frequency units, the anisotropy is also described in frequency units, using the symbol $\omega_0\delta$, making the simulations independent of the Larmor frequency.

Figure 2 simulates of the effect of changing the duration of an RF ramp through the $\omega_1 = 2\omega_r$ recoupling condition, by plotting the resulting transverse magnetization against $\omega_0\delta$. The RF amplitude is ramped from 30 to 50 kHz on a single ^{13}C spin, with $\eta = 1$, undergoing 20 kHz MAS. The results are normalized to the full transverse magnetization after a ramp on a spin with zero anisotropy. The results show, as expected, that increasing the duration of the ramp increases the efficiency of inversion. The simulation for a 20 ms ramp shows that when $\omega_0\delta > 5$ kHz more than 90% of the magnetization can be inverted. The inversion is less efficient for shorter ramps, but even a 2 ms ramp can achieve more than 70% inversion when $\omega_0\delta > 8$ kHz. The duration of the ramp can be used as a method to choose which CSA values are inverted

and which are not. At larger values of $\omega_0\delta$ the efficiency of inversion decreases because $\Delta\omega_1$ is no longer greater than $5c_{eff}$, and therefore increasing amounts of magnetization are lost during the initial and final projections.

The simulations in Figure 3 demonstrate the effect of varying the MAS frequency while using a constant ramp rate. Since the ramp extends from $1.5\omega_r$ to $2.5\omega_r$, the duration of the ramp must be extended as the MAS frequency increases in order to maintain a constant ramp rate. The simulations show the result on a single ^{13}C spin, with $\eta = 1$, by plotting the resulting transverse magnetization against the anisotropy. The behavior of each plot is nearly identical for small CSAs since the adiabaticity factor, Q, is similar for each of the ramps in this limit. The deviations that arise as the CSAs become larger are again due to losses during the initial and final projections of the spin polarization onto the Hamiltonian. These projections are minimized with larger ramps.

4. Results

Figure 4 shows the experimental result of changing the magnitude of the RF amplitude ramp after CP on a sample of [U-^{13}C, ^{15}N] L-tryptophan spinning at 22 kHz in a static magnetic field of 9.4 Tesla. After CP, the RF field amplitude was ramped down from 56.5 kHz (at time zero) to a final value of 31.5 kHz over a period of 2 ms. the ramp was interrupted at fixed intervals and ^{13}C spectra acquired. Thus, in Figure 4, the time axis corresponds to magnitude of the ramp. In essence, it demonstrates the behavior of the ^{13}C magnetization during a CSA recoupling experiment. We can see that the ramp has little effect on the magnetization before the $2\omega_r$ recoupling condition (roughly midway through the ramp) whereas after the midpoint of the ramp, signals from ^{13}C sites with a large CSA are inverted while signals from ^{13}C sites with small CSA tensors are attenuated but not inverted. The nature of this attenuation of spins with small CSAs near the CSA recoupling condition supports our earlier interpretation that the spins experience a small flip angle pulse near the recoupling condition while being spin-locked along I_x at all other times.

Figure 5 demonstrates the effect of changing the ramp rate on a sample of [U-^{13}C, ^{15}N] N-*acetyl*-valyl-leucine (VL) plotted against the duration of an RF ramp of 25 kHz, centered at the $\omega_1 = 2\omega_r$ CSA recoupling condition. The spectra were recorded at $\omega_r/2\pi = 22$ kHz ramping down from 56.5 kHz to 31.5 kHz in a static magnetic field strength of 9.4 Tesla. The duration of the sweep was varied from 0 to 4.5 ms.. While fast passage through the CSA recoupling condition does produce a noticeable effect, slowing down the sweep rate to less than 2.5 MHz/sec leads to an increase in the efficiency of inversion demonstrating the adiabatic nature of the inversion process. Figures 4 and 5 demonstrate that the carbon sites separate into two groups. Either the CSA tensor is large enough to cause inversion (carbonyl and aromatic sites) or it is not (aliphatic sites). Literature values for chemical shift tensors of amino acids [15], show that it is the disparity in the magnitude of the CSA, between aliphatic sites on one hand and aromatic and carbonyl sites on the other, that enables us to invert one set without inverting the other.

5. Chemical shift anisotropy selective inversion during cross-polarization

The pulse sequence (shown in Figure 1b) used to generate Figures 4 and 5 explicitly separates the initial cross-polarization period from the CSA recoupling period. However, it is possible to combine these two periods into a modification of the amplitude swept CP experiment [16, 17]. Amplitude swept or ramped CP can either be thought of as a method of reducing the instrumental imperfections such as RF inhomogeneity [16, 18] or as a method of improving the polarization transfer via Adiabatic Passage Hartmann-Hahn (APHH) CP [17]. The theoretical gain of the APHH CP compared to conventional CP in large spin systems (I_nS) has been investigated. It was shown that APHH CP should outperform non-ramped CP by a factor

of close to two [19]. This gain is predicted to occur when the width of the ramp is approximately equal to or greater than the MAS frequency.

There are 4 separate choices for implementation of ramped CP. The RF ramp can be applied to either channel, and RF power during the ramp can either increase or decrease. These choices can produce different effects.

Figure 6 shows effect of changing the direction of an RF amplitude sweep through a CSA rotary resonance condition during ramped CP on ^{13}C spectra of [U-^{13}C,^{15}N] N-*formyl* MLF-OH spinning at 31 kHz in a static magnetic field of 17.6 Tesla. Notice that there was no change in the magnitude of the RF amplitude sweep in Figure 6, only the direction. In order to produce CSA selective inversion during ramped CP, significant magnetization must have been built up via CP before the RF amplitude reaches the CSA recoupling condition. That is, the sweep must pass through a CP matching sideband [20] before reaching the CSA recoupling condition, and therefore the inversion only occurs with an amplitude sweep in the correct direction.

This combination of CSA selective inversion and CP can be put to use. In Figure 7 we show a 2D Proton Driven Spin Diffusion (PDSD) [21] ^{13}C–^{13}C correlation spectrum of [U-^{13}C, ^{15}N] N-*formyl* MLF-OH under similar conditions as Figure 6, in which the carbonyl and aromatic region were inverted with respect to the aliphatic region, simply by adjusting the parameters of ^{13}C RF ramp during the initial cross-polarization. Cross-peaks arising from the inverted spins appear negative (green) while those arising from non-inverted spins appear positive (red). This form of selective inversion can be achieved without increasing the duration of the pulse sequence, and/or without the addition of additional pulse sequence elements such as frequency selective soft pulses. This technique could also be thought of as the basis of a method of measuring CSAs in 2D correlation spectra at high MAS frequencies.

6. Conclusions

We have examined the process of chemical shift anisotropy selective inversion in solids undergoing MAS, both in theory and in practice. We have shown that it is relatively easy to invert carbonyl and aromatic sites (both of which have high anisotropies) while merely attenuating the aliphatic sites (which have low anisotropies) using ramps with various durations between 2 and 5 ms at static magnetic fields between 9.4 and 17.6 Tesla. Since the adiabaticity of the CSA inversion depends on the size of the CSA, performing these experiments at higher magnetic fields should allow sites with smaller CSA to be inverted. Higher MAS frequencies should also be beneficial, as it permits a larger range of sweep sizes and rates. The combination of higher static magnetic fields and higher MAS frequencies should allow for greater control of selective inversion as a function of CSA.

CSA selective inversion can be combined with CP by sweeping the RF amplitude through a sideband of the CP matching profile before extending the sweep to match a multiple of the spinning frequency. In this situation, the results are dependent not only upon the magnitude of the RF amplitude sweep but also the direction. In conditions where the CP matching power is near a multiple of the spinning frequency, this combination of CP and CSA inversion may be encountered inadvertently while attempting to perform ramped CP.

Since protons generally have small CSA values it might seem preferable to apply the amplitude ramp to the proton channel during ramped CP experiments in order to avoid CSA recoupling. However, with the increasing use of proton Larmor frequencies of 900 MHz and above, a proton CSA of 10 PPM produces a $\omega_0\delta$ of 9 kHz. The simulations shown in Figures 2 and 3 demonstrate that this is quite large enough to cause CSA inversion. While reversing the direction of RF amplitude sweep can often reduce these effects, the only safe way to prevent CSA recoupling is to avoid all recoupling conditions (except CP) on both channels.

Acknowledgments

The research was supported by the National Institutes of Biomedical Imaging and Bioengineering through grants EB-003151 and EB-002026. We would like to thank Dr. M. Veshtort, and Dr. G. De Paepe for simulating discussions. We would also like to give special thanks to an unknown referee who alerted us to the work cited in reference [3] which was previously unknown to us.

References

1. Alexander S. Spin-echo method for measuring relaxation times in two-line NMR spectra. Rev Sci Instrum 1961;32:1066–1067.
2. Gan Z, Grant DM, Ernst RR. NMR chemical shift anisotropy measurements by RF driven rotary resonance. Chem Phys Lett 1996;254:349–357.
3. Asakawa N. Determination of small shielding anisotropy by adiabatically ramped spin-locking NMR and ab initio chemical shielding calculation: L-alanine methyl carbon. J Mol Struc-Theochem 2004;675:29–35.
4. Bennett, AE.; Griffin, RG.; Vega, S. Recoupling of homo- and heteronuclear dipolar interactions in rotating solids, Vol. 33 of NMR Basic Principles and Progress, Solid-State NMR IV. Springer-Verlag; Berlin: 1994. p. 1-77.
5. Meier, BH. Polarization transfer and spin diffusion in solid-state NMR. In: Warren, WS., editor. Advances in Magnetic and Optical Resonance. Vol. 18. Academic Press; New York: 1994. p. 1-116.
6. Bennett AE, Rienstra CM, Griffiths JM, Zhen WG, Lansbury PT, Griffin RG. Homonuclear radio frequency-driven recoupling in rotating solids. J Chem Phys 1998;108:9463–9479.
7. Ishii Y, Ashida J, Terao T. 13C-1H Dipolar recoupling dynamics in 13C multiple-pulse solid-state NMR. Chem Phys Lett 1995;246:439–445.
8. Haeberlen, U. High resolution NMR in solids, selective averaging. Academic Press; New York: 1976.
9. Verel R, Meier BH. Polarization-transfer methods in solid-state magic-angle-spinning NMR: Adiabatic CN pulse sequences. ChemPhysChem 2004;5:851–862. [PubMed: 15253311]
10. Kupce E, Freeman R. Stretched adiabatic pulses for broadband spin inversion. J Magn Reson 1995;117A:246–256.
11. Oas TG, Griffin RG, Levitt MH. Rotary resonance recoupling of dipolar interactions in solid-state nuclear magnetic resonance spectroscopy. J Chem Phys 1988;89:692–695.
12. Ernst M, Samoson A, Meier BH. Decoupling and recoupling using continuous-wave irradiation in magic-angle-spinning solid-state NMR: A unified description using bimodal Floquet theory. J Chem Phys 2005;123:064102.
13. Lewandowski JR, De Paepe G, Griffin RG. Proton assisted insensitive nuclei cross polarization. J Am Chem Soc 2007;129:728–729. [PubMed: 17243786]
14. Veshtort M, Griffin RG. SPINEVOLUTION: A powerful tool for the simulation of solid and liquid state NMR experiments. J Magn Reson 2006;178:248–282. [PubMed: 16338152]
15. Ye C, Fu R, Hu J, Ding S. Carbon-13 chemical shift anisotropies of solid amino acids. Magn Reson Chem 1993;31:699–704.
16. Petersen OB, Wu X, Smith SS. Enhancement of CP-MAS signals by variable-amplitude cross polarization. Compensation for inhomogeneous B_1 fields. J Magn Reson 1994;106A:127–131.
17. Hediger S, Meier BH, Ernst RR. Adiabatic passage Hartmann-Hahn cross polarization in NMR under magic angle sample spinning. Chem Phys Lett 1995;240:449–456.
18. Paulson EK, Martin RW, Zilm KW. Cross polarization, radio frequency field homogeneity and circuit balancing in high field solid state NMR probes. J Magn Reson 2004;171:314–323. [PubMed: 15546758]
19. Hodgkinson P, Pines A. Cross-polarization efficiency in I_nS systems using adiabatic RF sweeps. J Chem Phys 1997;107:8742–8751.
20. Stejskal EO, Schaefer J, Waugh JS. Magic-angle spinning and polarization transfer in proton-enhanced NMR. J Magn Reson 1977;28:105–112.
21. Szeverenyi NM, Sullivan MJ, Maciel GE. Observation of spin exchange by two-dimensional Fourier transform 13C cross polarization-magic-angle spinning. J Magn Reson 1982;47:462–475.

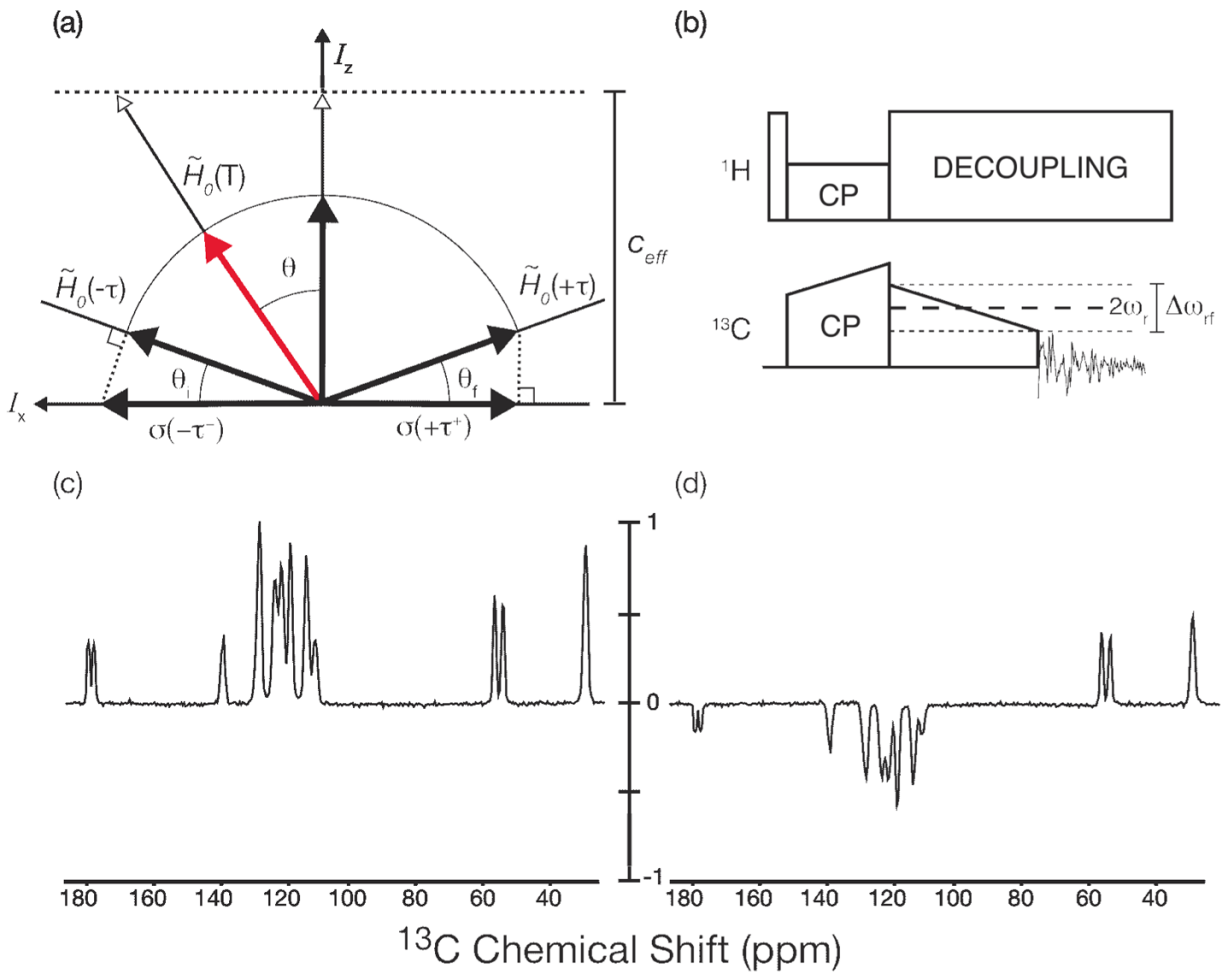

Figure 1.

(a) Depiction of an adiabatic sweep of the Hamiltonian from I_x to $-I_x$. The initial spin state $\sigma(-\tau^-)$ is projected from I_x onto the Hamiltonian as the RF ramp begins. The polarization is spin-locked along the Hamiltonian and then dragged through the CSA recoupling axis to $-I_x$ as the RF field is ramped through the CSA recoupling condition. In order for the inversion to occur, the angular sweep rate of the Hamiltonian, $d\theta/dT$, must remain small relative to the size of the Hamiltonian (adiabatic condition), and the initial and final projection angles (θ_i and θ_f) must remain small. (b) The pulse sequence used to demonstrate adiabatic CSA recoupling. (c) ^{13}C CPMAS spectrum of [U-^{13}C, ^{15}N] L-tryptophan. (d) $\omega_1 = 2\omega_r$ CSA recoupled spectrum of [U-^{13}C, ^{15}N] L-tryptophan. Both spectra (c) and (d) are plotted on the same absolute intensity scale and their intensities are directly comparable.

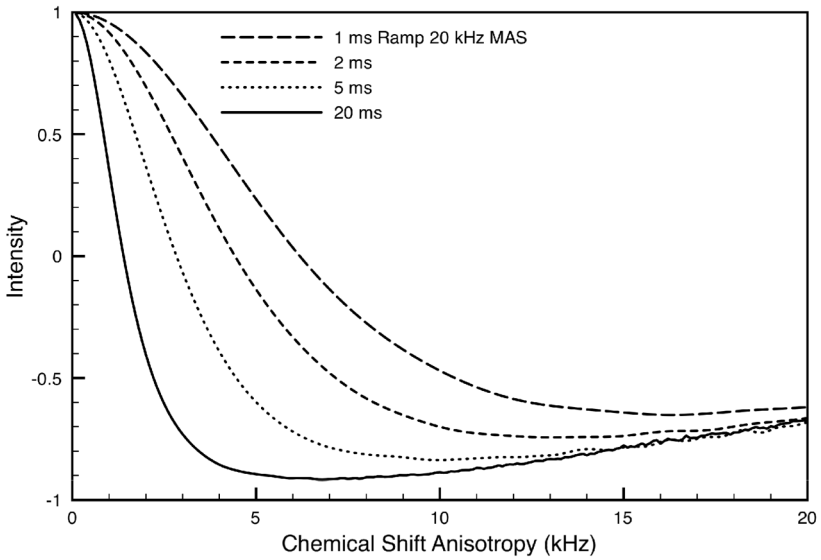

Figure 2.

Numerical simulations of the effect of the duration of an RF amplitude ramp on the transverse magnetization plotted against the CSA in frequency units with a fixed asymmetry (η = 1) at the $\omega_1 = 2\omega_r$ recoupling condition. The RF amplitude was ramped from 30 to 50 kHz on a single ^{13}C spin undergoing 20 kHz MAS. The simulations were carried out with SPINEVOLUTION 3.3.3 [14]

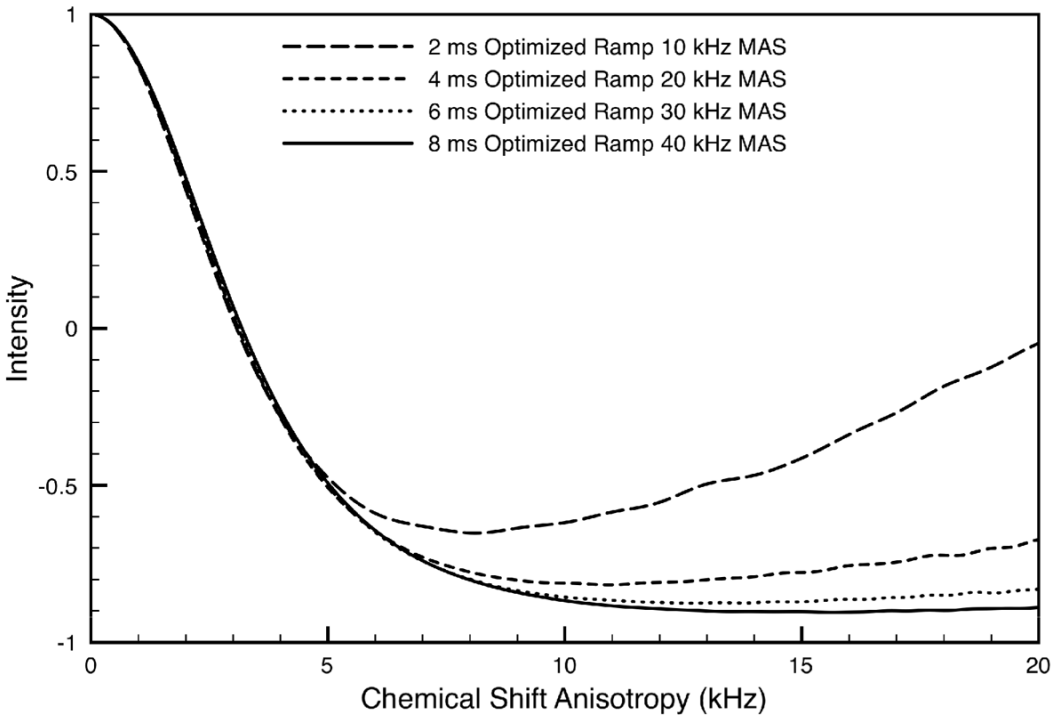

Figure 3.

Numerical simulations of the effect of varying the MAS frequency on the transverse magnetization when plotted against the CSA ($\omega_0\delta$) with a constant ramp rate and a fixed asymmetry ($\eta = 1$) at the $\omega_1 = 2\omega_r$ recoupling condition. The RF ramp rate was fixed at 5 kHz/ms and ramped from $1.5\omega_r$ to $2.5\omega_r$ (optimized ramp). The simulations were carried out with SPINEVOLUTION 3.3.3 [14] using a single ^{13}C spin.

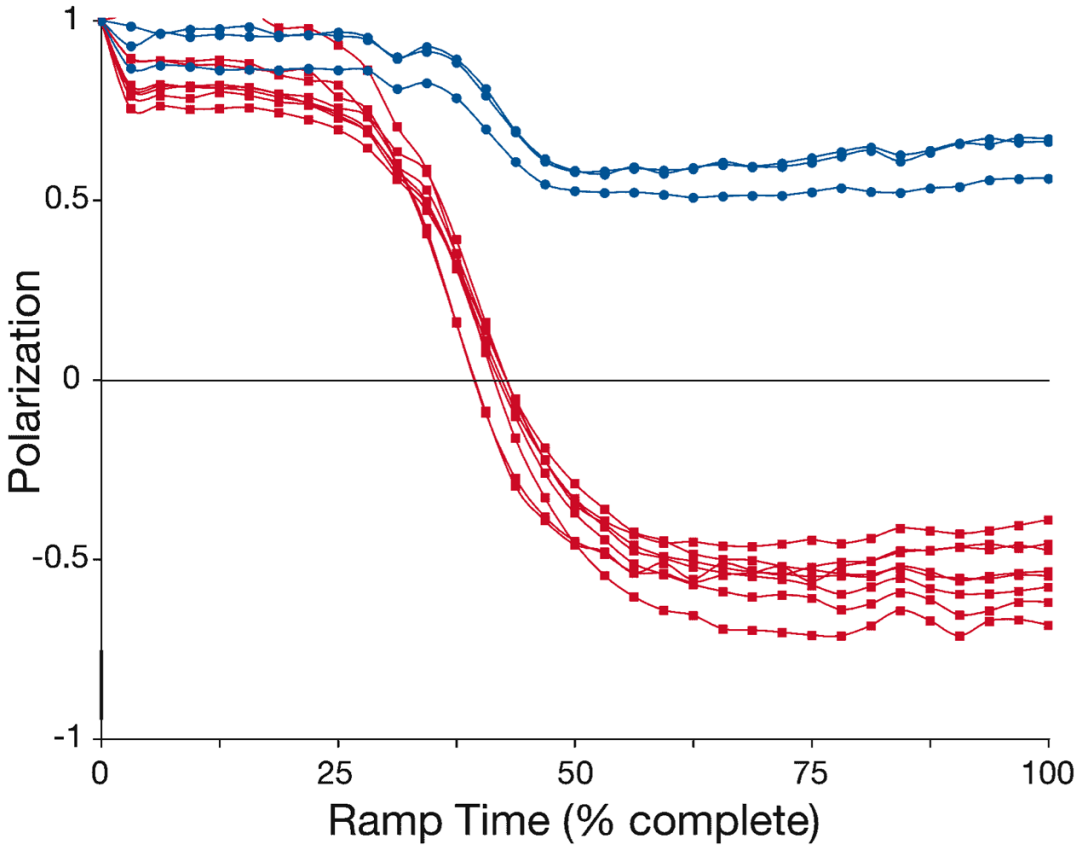

Figure 4.

Experimental results showing the peak heights of the carbon sites of [U-^{13}C, ^{15}N] L-tryptophan at various points during a CSA-selective inversion ramp. The aliphatic sites (shown in blue) remain positive while the carbonyl and aromatic sites (shown in red) are inverted as the ramp passes through the $\omega_1 = 2\omega_r$ recoupling condition. The spectra were measured at $\omega_r/2\pi = 22$ kHz MAS in a static magnetic field strength of 9.4 Tesla during a 2 ms ramp from 56.5 to 31.5 kHz.

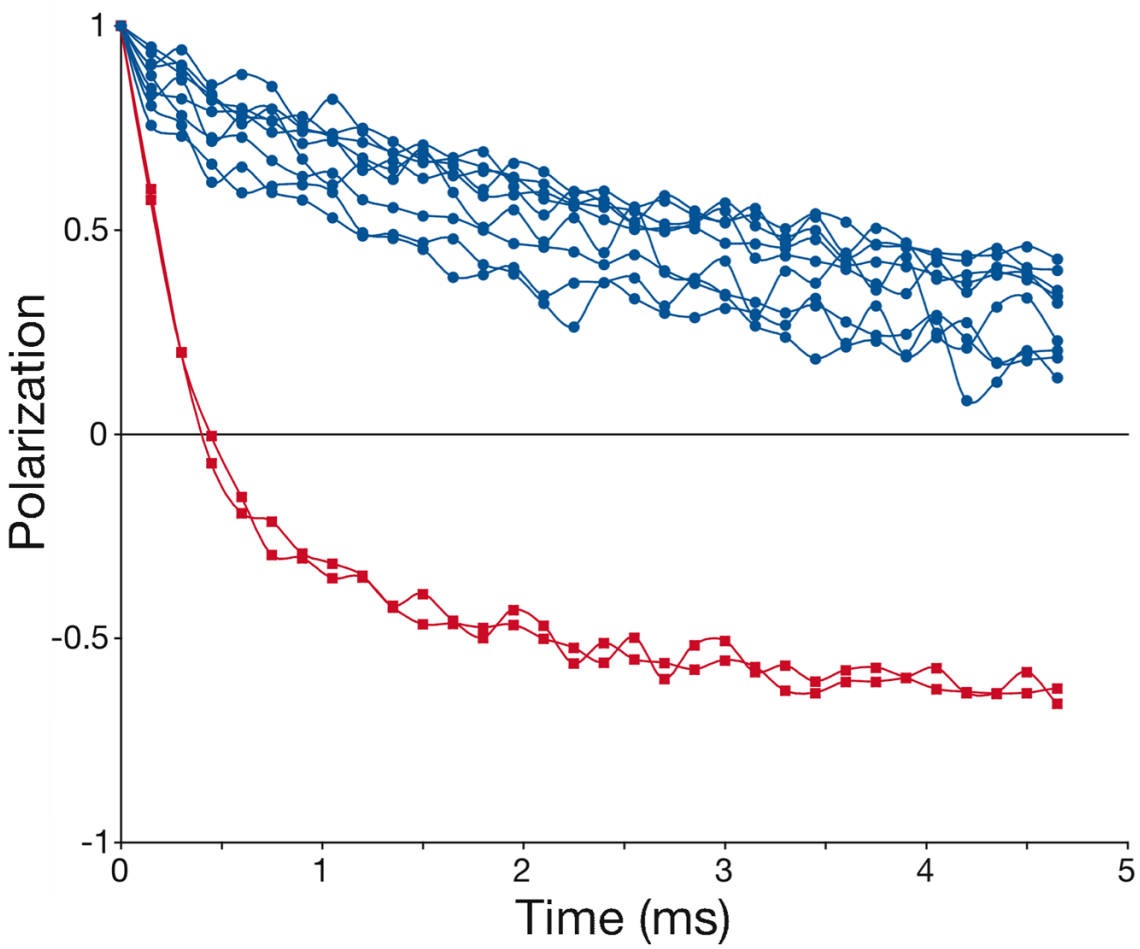

Figure 5.

Experimental data showing the peak heights of the carbon sites of [U-^{13}C, ^{15}N,] N-*acetyl*-valyl-leucine (VL) plotted against the duration of an RF amplitude sweep range of 25 kHz, centered at the $\omega_1 = 2\omega_r$ CSA recoupling condition. The aliphatic carbons (shown in blue) are not inverted by the ramp even at longer ramp times, while the carbonyl carbons (shown in red) are inverted with increasing efficiency as the duration of the ramp increases (decreasing ramp rate). The spectra were recorded at $\omega_r/2\pi$ = 22 kHz ramping down from 56.5 kHz to 31.5 kHz in a static magnetic field strength of 9.4 Tesla.

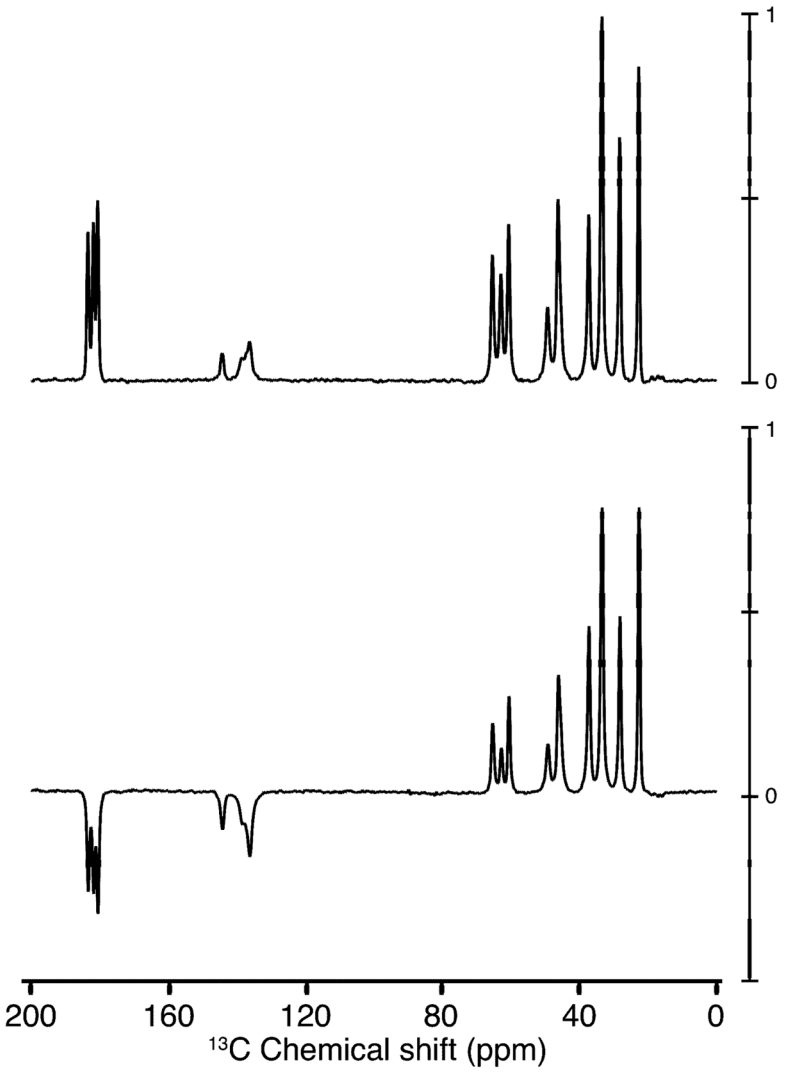

Figure 6.

(Top) Ramped CP spectrum of [U-^{13}C, ^{15}N] N-*f*-MLF-OH (MLF) spinning at 31 kHz in a static magnetic field strength of 17.6 Tesla with a ^{13}C RF amplitude sweep passing through the $\omega_1 = 2\omega_r$ CSA recoupling condition before passing through the CP sideband, resulting in an all-positive spectrum. (Bottom) Ramped CP spectrum of MLF as above except the direction of the sweep was reversed to pass first through the CP sideband and then through the n =2 recoupling condition, leading to inversion of peaks with large CSA tensors. Both spectra are plotted on the same absolute intensity scale, and their intensities are directly comparable.

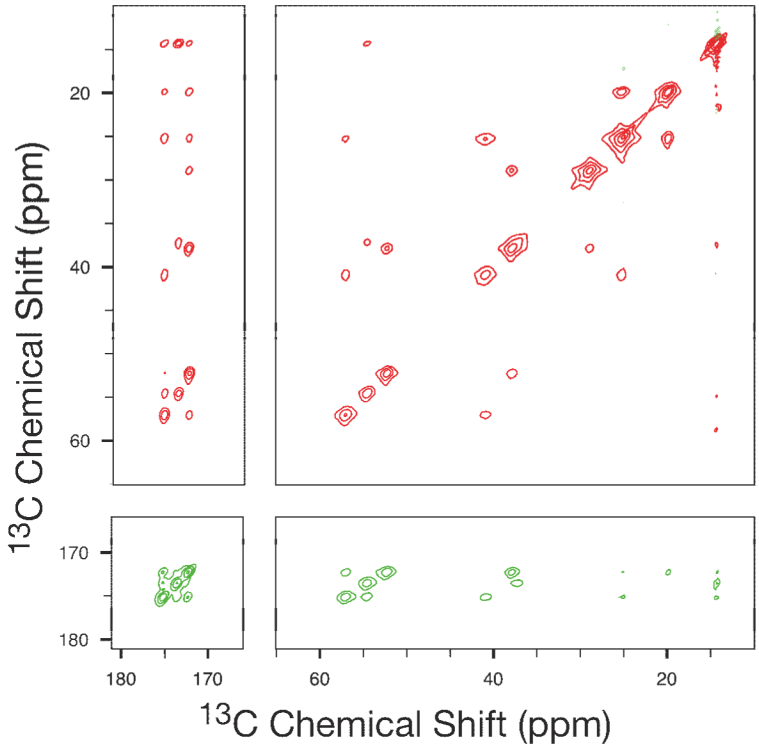

Figure 7.

2D ^{13}C – ^{13}C correlation spectrum of [U-^{13}C, ^{15}N] N-*f*-MLF-OH combined with CSA selective inversion. The spectrum was recorded at a static magnetic field strength of 17.6 Tesla with 31 kHz MAS using Proton Driven Spin Diffusion [21] and a mixing time of 40 ms.. The ^{13}C RF amplitude ramp passes first through the CP sideband and then through the $\omega_1 = 2\omega_r$ recoupling condition, resulting in the inversion of peaks with large CSA values. Cross-peaks arising from the inverted spins appear negative (green) while those arising from non-inverted spins appear positive (red). The aromatic region was also inverted but is not displayed as it contains few cross-peaks.